Influence of Tropical Tropopause Layer Cooling on Atlantic Hurricane Activity

KERRY EMANUEL AND SUSAN SOLOMON

Program in Atmospheres, Oceans, and Climate, Massachusetts Institute of Technology, Cambridge, Massachusetts

DORIS FOLINI

Institute for Atmospheric and Climate Science, ETH Zurich, Zurich, Switzerland

SEAN DAVIS

NOAA/Earth System Research Laboratory, Chemical Sciences Division, and Cooperative Institute for Research in Environmental Sciences, University of Colorado at Boulder, Boulder, Colorado

CHIARA CAGNAZZO

Euro-Mediterranean Center for Climate Change, Bologna, and Istituto di Scienze dell'Atmosfera e del Clima, ISAC-CNR, Rome, Italy

(Manuscript received 30 April 2012, in final form 20 August 2012)

ABSTRACT

Virtually all metrics of Atlantic tropical cyclone activity show substantial increases over the past two decades. It is argued here that cooling near the tropical tropopause and the associated decrease in tropical cyclone outflow temperature contributed to the observed increase in tropical cyclone potential intensity over this period. Quantitative uncertainties in the magnitude of the cooling are important, but a broad range of observations supports some cooling. Downscalings of the output of atmospheric general circulation models (AGCMs) that are driven by observed sea surface temperatures and sea ice cover produce little if any increase in Atlantic tropical cyclone metrics over the past two decades, even though observed variability before roughly 1970 is well simulated by some of the models. Part of this shortcoming is traced to the failure of the AGCMs examined to reproduce the observed cooling of the lower stratosphere and tropical tropopause layer (TTL) over the past few decades. The authors caution against using sea surface temperature or proxies based on it to make projections of tropical cyclone activity as there can be significant contributions from other variables such as the outflow temperature. The proposed mechanisms of TTL cooling (e.g., ozone depletion and stratospheric circulation changes) are reviewed, and the need for improved representations of these processes in global models in order to improve projections of future tropical cyclone activity is emphasized.

1. Introduction

Various metrics of North Atlantic tropical cyclone activity show large increases over the past two decades. For example, tropical cyclone power dissipation [the sum over the season and the lifetime of each storm of its maximum surface wind speed cubed; Emanuel (2005)] has increased in concert with the sea surface temperature of the tropical North Atlantic main development region (MDR) (6°–18°N, 20°–60°W) since the 1980s (Fig. 1).

The high correlation ($r^2 = 0.77$) between the two time series is remarkable for two entirely independent geophysical measurements. The actual (nonnormalized) power dissipation has roughly doubled since 1990, while the (nonnormalized) sea surface temperature has increased by only about 0.5°C during this period. Were this apparent sensitivity to continue into a projected 2°–3°C increase in tropical sea surface temperatures owing to global warming, the implications would be dire (Knutson et al. 2010). It is the aim of this paper to explore the physical causes of the large upswing in Atlantic tropical cyclone power in the past two decades, focusing on the role of temperature changes in the tropical tropopause layer (TTL). Here we confine our attention to the North

Corresponding author address: Kerry Emanuel, Room 54-1814, MIT, 77 Massachusetts Avenue, Cambridge, MA 02138.
E-mail: emanuel@mit.edu

DOI: 10.1175/JCLI-D-12-00242.1

Atlantic region for three primary reasons. First, records of tropical cyclone activity (including intensity) there are of higher quality and longer duration than anywhere else. Second, as we will show presently, variability of North Atlantic tropical cyclone activity appears to be more controlled by thermodynamic variability than elsewhere. Finally, as we will show, there are data that suggest that cooling of the tropical tropopause layer is more pronounced over the tropical North Atlantic than in many other parts of the tropics. Thus, the signal whose influence we here seek to elucidate is probably stronger in the North Atlantic than elsewhere.

2. Thermodynamic influences on tropical cyclones

We first note that, in spite of the high correlation between tropical cyclone power and sea surface temperature evident in Fig. 1, sea surface temperature plays no well-defined direct role in any existing theory of tropical cyclones, even though it is widely used in empirical relationships for genesis and storm intensity and by forecasters trying to predict genesis and intensity change. Physically, the atmosphere responds to the ocean mostly through radiative fluxes, which depend, among other things, on the ocean temperature relative to the temperature at various levels in the atmosphere, and on turbulent enthalpy fluxes, which depend on near-surface wind speed and on the difference between the saturation enthalpy of the sea surface and the actual enthalpy of the boundary layer. It is the difference that matters, not the absolute value of the sea surface temperature.

We identify three thermodynamically sensitive quantities of potential significance to tropical cyclones: 1) the general incidence of moist convection, 2) a nondimensional measure of midtropospheric humidity, and 3) the potential intensity, which depends on both the enthalpy jump between the atmosphere and ocean and the temperature difference between the ocean and the tropopause.

One metric of moist convection is the cloud-base updraft mass flux M_u averaged over an ensemble of convective clouds. According to the boundary layer quasi-equilibrium hypothesis of Raymond (1995), the convective and large-scale downdrafts into the subcloud layer must, on average, balance surface enthalpy fluxes in order that there are no large tendencies of entropy in the subcloud layer. Assuming that both convective downdrafts and large-scale subsidence into the subcloud layer both transport a value of moist static energy h_m characteristic of the middle troposphere, Emanuel (1995) showed that the updraft mass flux is given by

$$M_u = \gamma w + C_k|\mathbf{V}|\frac{h_0^* - h_b}{h_b - h_m}, \tag{1}$$

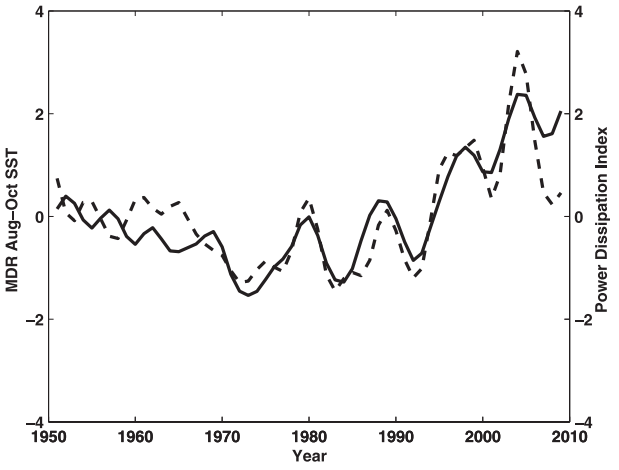

FIG. 1. Seasonally accumulated tropical cyclone power dissipation (dashed) and sea surface temperature (from the Hadley Center) averaged over the Atlantic main development region (6°–18°N, 20°–60°W) and over the period August–October (solid), using data for the period 1949–2010. Tropical cyclone wind speeds are from the National Hurricane Center "best track" data, but using wind speed corrections according to Emanuel (2005) over the period 1949–70. Sea surface temperature is from the Hadley Center (HadISST1). Both series have first been zero-centered and normalized by their respective standard deviations and then smoothed using a 1–3–4–3–1 filter.

where w is the large-scale vertical velocity at a characteristic altitude in the middle troposphere, γ is a scaling factor such that γw represents the large-scale vertical velocity at the top of the boundary layer, C_k is the nondimensional surface exchange coefficient for enthalpy at a reference altitude in the surface layer, $|\mathbf{V}|$ is the wind speed at that reference altitude, h_0^* is the saturation moist static energy of the sea surface, and h_b is the boundary layer moist static energy. The derivation of (1) assumes that there is no horizontal advection of moist static energy in the boundary layer and neglects radiative cooling integrated through the depth of the boundary layer. In the free troposphere there must be, on average, a balance between radiative cooling and the warming due to subsidence between clouds. This balance may be expressed as

$$(M_u - M_d - w)S = \dot{Q}_{\mathrm{rad}}, \tag{2}$$

where M_d is the net convective downdraft mass flux (defined positive downward), $\dot{Q}_{\mathrm{rad}}$ is the radiative cooling rate, and S is the static stability, defined as

$$S = c_p(\Gamma_d - \Gamma_m),$$

where c_p is the heat capacity at constant pressure and Γ_d and Γ_m are the dry and moist adiabatic lapse rates,

respectively. If we assume that the downdraft mass flux depends on the updraft mass flux according to $M_d = (1 - \varepsilon_p)M_u$, where ε_p is the precipitation efficiency (Emanuel 1995), then using this and eliminating w between (1) and (2) yields

$$M_u = \frac{1}{1 - \gamma\varepsilon_p}\left[\frac{C_k|\mathbf{V}|(h_0^* - h^*)}{h^* - h_m} - \frac{\gamma\dot{Q}_{\rm rad}}{S}\right]. \quad (3)$$

In writing (3) we have also assumed that convective regions are nearly neutrally stable to moist convection so that $h_b = h^*$, where h^* is the saturation moist static energy of the troposphere that, owing to convective neutrality, is nearly constant with altitude and, owing to horizontal temperature gradients being very weak in the tropical troposphere, is nearly constant in the horizontal as well. We have also neglected horizontal entropy advection in the boundary layer and in the free troposphere.

It is apparent from (3) that convection depends on many environmental factors, including the saturation deficit of the middle troposphere (denominator of the first term in brackets), radiative cooling, precipitation efficiency, near-surface wind speed, and the saturation moist static energy of the sea surface relative to that of the troposphere. This last factor is also important in the expression for potential intensity $V_{\rm pot}$ of tropical cyclones (e.g., Bister and Emanuel 1998):

$$V_{\rm pot}^2 = \frac{C_k}{C_D}\frac{T_s - T_o}{T_o}(h_0^* - h^*), \quad (4)$$

where C_D is the drag coefficient, and we have once again equated the boundary layer moist static energy with the saturation moist static energy of the free troposphere.[1] In (4) T_s is the sea surface temperature and T_o is the "outflow temperature," which is approximately the temperature near the ambient tropopause (Emanuel and Rotunno 2011). The direct dependence of potential intensity on sea surface temperature T_s in (4) is weak; a 0.5°C increase would yield an increase of potential intensity of about 0.2 m s^{-1}. Most of the dependence enters through the factor $h_0^* - h^*$, which also appears in the expression for the convective mass flux, (3). This may be thought of as dependent on the temperature of the ocean surface relative to that of the free troposphere.

It should also be mentioned that simple models of tropical cyclones suggest that the nondimensional quantity χ defined by

$$\chi \equiv \frac{h_0^* - h^*}{h^* - h_m}, \quad (5)$$

which also appears in (3), has an important effect on the genesis and development of tropical cyclones (Emanuel et al. 2008). Specifically, larger values of χ are conducive to more frequent storms [and, through (3), to more convection]. As argued by Emanuel et al. (2008), global warming should lead to decreasing χ since the numerator of (5), which scales as surface enthalpy fluxes, increases only slowly with increasing greenhouse gas content, while the denominator of (5) increases more rapidly, scaling with the Clausius–Clapeyron relation. This, together with (4), suggests that global warming should lead to less frequent but more intense tropical cyclones.

We now return to the question of the remarkable increase of Atlantic tropical cyclone power and sea surface temperature and the correlation between them. Examining (3)–(5), we note that the primary quantities whose variation one might expect to affect tropical cyclone (TC) activity are $h_0^* - h^*$, $h^* - h_m$, $|\mathbf{V}|$, and T_o. We would expect a high correlation between metrics of TC activity and sea surface activity when all or most of these are correlated with sea surface temperature, especially if the nonthermodynamic effects on tropical cyclones such as wind shear are also correlated with sea surface temperature. Table 1 shows the correlation coefficients between sea surface temperature and these various quantities, as well as the associated P values for three TC-producing regions. Only in the North Atlantic region are all of the correlations highly significant[2] and these high correlations among the thermodynamic predictors are consistent with the high correlation between tropical cyclone metrics (such as power dissipation) and sea surface temperature in the North Atlantic. Not surprisingly, the Atlantic is the only region of the three in which tropical cyclone power dissipation is significantly correlated with potential intensity [at least according to National Centers for Environmental Prediction (NCEP)–National Center for Atmospheric Research (NCAR) reanalysis data], so it is a good place to examine the influence of outflow temperature, which affects potential intensity. In the following, we examine in detail

[1] The validity of (4) has been challenged by Smith et al. (2008) and examined by others (e.g., Bryan and Rotunno 2009), but an alternative formulation has not been proposed.

[2] But correlations involving the outflow temperature using NCEP–NCAR reanalysis data are dubious, as described in the next section.

TABLE 1. Correlations between SST and power dissipation index (PDI), as well as various quantities that appear in (3)–(5) and with the 850–250-hPa wind shear (last column): *P* values are indicated in parentheses. All quantities, including SST, have been calculated from NCEP–NCAR reanalysis data over the period 1979–2010, and have been smoothed using a 1–3–4–3–1 filter. The outflow temperature was calculated using the algorithm presented in Bister and Emanuel (2002). The averaging regions and months are Atlantic: 6°–18°N, 20°–60°W, August–October; eastern North Pacific: 5°–16°N, 90°–170°W, July–September; and western North Pacific: 5°–15°N, 130°E–180°, July–November.

	PDI	$h_0^* - h^*$	$\frac{1}{h^* - h_m}$	$\lvert\mathbf{V}\rvert$	T_o	$\lvert\Delta\mathbf{V}\rvert_{250-850}$
Atlantic	0.85 (0.000)	0.892 (0.000)	−0.478 (0.010)	−0.899 (0.000)	−0.859 (0.000)	−0.719 (0.000)
Eastern North Pacific	0.500 (0.007)	0.892 (0.000)	−0.189 (0.335)	−0.212 (0.278)	−0.148 (0.452)	−0.453 (0.016)
Western North Pacific	−0.177 (0.368)	0.730 (0.000)	0.558 (0.007)	−0.019 (0.482)	−0.839 (0.000)	0.349 (0.069)

the contribution to increasing North Atlantic hurricane power from decreasing outflow temperature.

3. The influence of outflow temperature on trends in Atlantic potential intensity

To further examine the effects of various factors on potential intensity, we begin by taking the logarithm of (4):

$$2\log(V_{\text{pot}}) = \log\left(\frac{C_k}{C_D}\right) + \log\left(\frac{T_s - T_o}{T_o}\right) + \log(h_0^* - h^*). \tag{6}$$

Figure 2 shows the variation with time of the last two factors in (6), averaged over the MDR (6°–18°N, 20°–60°W) using the algorithm of Bister and Emanuel (2002) driven by the NCEP–NCAR reanalysis as an example. [Note that, according to the Bister and Emanuel algorithm, temperature changes that do not affect either boundary layer entropy or the outflow temperature (approximately the temperature of the tropopause) do not affect potential intensity. Thus, for example, any temperature changes in the upper troposphere well below the tropical tropopause layer (whether real or spurious, see below) do not change potential intensity in any significant way.]

Sea surface temperature measurements in the tropical North Atlantic region have been accurate and robust over the period that we are concerned with here, so this contribution to changes in potential intensity is well characterized. If the NCEP–NCAR reanalysis is adopted, slightly more than half (56%) of the increase of potential intensity in the North Atlantic over the past 30 years is owing to an increase in thermodynamic efficiency, the second term on the right of (6). As discussed previously, virtually all of this comes from the decrease of outflow temperature; the increase in sea surface temperature contributes only about 7% to the increase in thermodynamics efficiency over this period. The increase

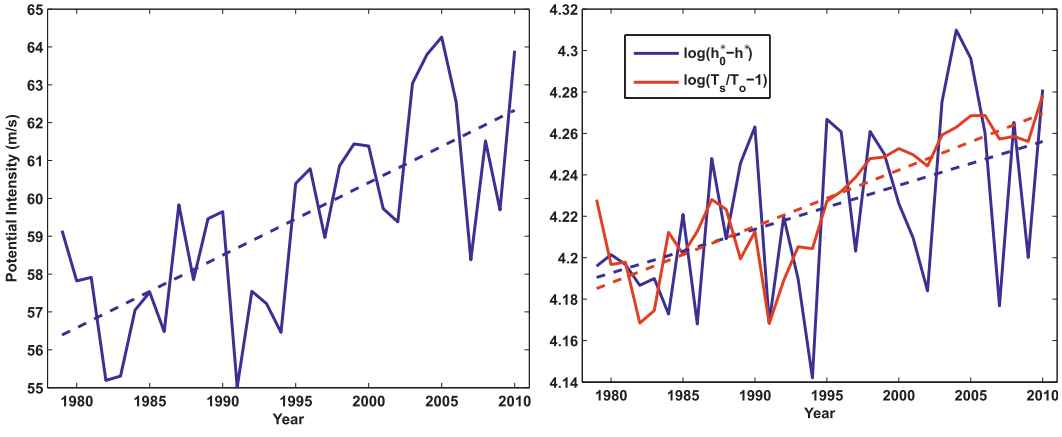

FIG. 2. (left) Potential intensity calculated from the algorithm of Bister and Emanuel (2002) averaged over the Atlantic main development region (6°–18°N, 20°–60°W) and over August–October, using NCEP–NCAR reanalysis data. The dashed line shows the linear regression slope. (right) Logarithms of the last two factors in (6): thermodynamic efficiency (red, with 4.75 added for ease of comparison) and surface thermodynamic disequilibrium (blue). Dashed lines show the regression slopes, calculated from NCEP–NCAR reanalysis data averaged over the Atlantic main development region (6°–18°N, 20°–60°W) and over August–October; outflow temperature calculated using the algorithm of Bister and Emanuel (2002).

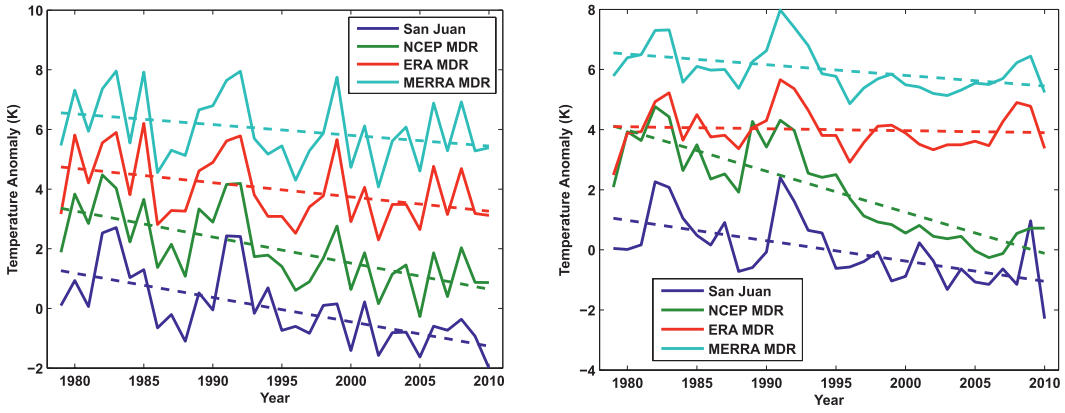

FIG. 3. August–October averaged temperature anomalies at (left) 70 hPa and (right) 100 hPa for the period 1979–2010: RATPAC station data at San Juan, Puerto Rico (blue); NCEP–NCAR reanalysis data (green); ERA-Interim reanalysis data (red); and MERRA reanalysis data (aqua) averaged over the region 6°–18°N, 20°–60°W are compared. Dashed lines show the linear regression slopes. The temperature anomalies are with respect to their respective means over the period of record, and 2 K has been added successively to each series for clarity.

in tropical cyclone activity downscaled from the NCEP–NCAR reanalyses reported by Emanuel et al. (2008) arises almost entirely from the increase in potential intensity; the 5% decline in wind shear over the period is too small to contribute much to the increase, and the other parameter important in the downscaling, χ, as given by (5), actually declines over the period. The magnitude of this contribution is certainly an overestimate because the NCEP–NCAR reanalysis cools the tropopause region excessively compared to soundings and Microwave Sounding Unit (MSU)-based analyses. Next we show that the quality and consistency of available temperature records and reanalysis has improved greatly in recent years, allowing a deeper examination of the robustness of cooling in the tropical tropopause region.

The reanalysis rendition of TTL temperatures depends upon observations by radiosondes and satellite radiometric measurements in certain wavenumber ranges. Some of the radiometric measurements are assimilated into reanalysis products. We next compare the NCEP–NCAR reanalysis temperatures at 100 and 70 hPa, averaged over the Atlantic MDR during August–October, to two other reanalysis products and to radiosonde temperatures at San Juan, Puerto Rico, the nearest quality-checked station with a long record for which Radiosonde Atmospheric Temperature Products for Assessing Climate (RATPAC-lite) data are available. These radiosonde data have been corrected for temporal inhomogeneity problems (Lanzante et al. 2003a,b). Although Puerto Rico is some distance from the Atlantic MDR, the stratification in the TTL and lower stratosphere coupled with the relatively low latitudes of the region ensure that the deformation radius will be comparatively large, so one might expect some correlation between the Puerto Rico and MDR temperatures at 100 and 70 hPa. Figure 3 compares the RATPAC Puerto Rico temperature anomalies averaged over both 0000 and 1200 UTC times and over the months August–October with MDR-averaged reanalysis data averaged over the same months. Besides the NCEP–NCAR reanalysis, we also compare with interim European Centre for Medium-Range Weather Forecasts Re-Analysis (ERA-Interim) (Dee et al. 2011) and Modern-Era Retrospective Analysis for Research and Applications (MERRA) (Rienecker et al. 2011) reanalysis data.

At 70 hPa the sonde and the three reanalysis products all show downward trends, although the MERRA and ERA trends are smaller than those of the San Juan radiosonde and the NCEP–NCAR reanalysis.[3] The effects of the two major volcanic eruptions during this period, El Chichón in 1982 and Mt. Pinatubo in 1991, are apparent at both 70 and 100 hPa. Of direct importance to the present work is the absence of significant cooling at 100 hPa in the ERA-Interim reanalysis. The San Juan radiosonde shows significant cooling, while the MERRA reanalysis cools but to a lesser degree. The NCEP–NCAR reanalysis cooling trend is somewhat larger than that at San Juan. The MERRA and ERA-Interim reanalyses (as well as two other reanalyses discussed in the next paragraph) agree quite well with each other and with the San Juan sounding when they are interpolated to the location of San Juan, indicating that the reanalyses are

[3] While the temperature at 70 hPa does not affect potential intensity, it is the lowest standard radiosonde level that can reasonably be assumed to be unaffected by vertical migrations of the TTL; thus it is useful to examine temperature tendencies there.

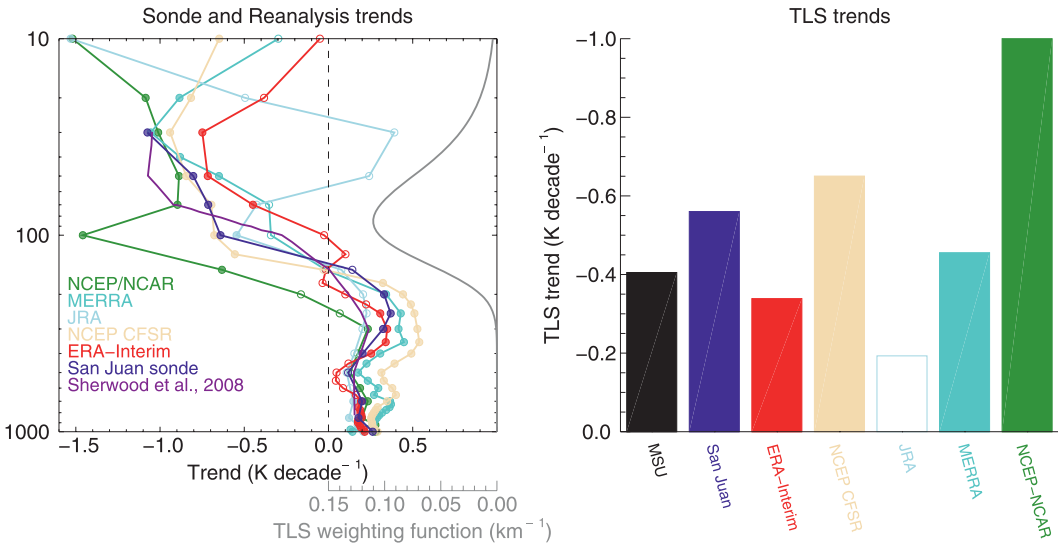

FIG. 4. (left) Vertical distributions of August–October MDR-averaged temperature trends (1979–2009) from five reanalyses and from the San Juan radiosonde, compared with annual mean tropical-wide temperature trends from wind-adjusted radiosonde data (Sherwood et al. 2008). Vertical weighting function of the MSU TLS channel shown at right. (right) Temperature trends from the MSU-weighted San Juan sounding and the five reanalyses, compared with MSU TLS data averaged over the MDR, August–October. The trend of the JRA-25 reanalysis is not significant at the 95% level, as indicated by the open bar.

more strongly constrained by the radiosonde data near the location of the sounding.

In Fig. 4, linear trends in temperature from the San Juan radiosonde and the three reanalysis products are compared with two other reanalyses: the Japanese Meteorological Agency (JMA) 25-yr Reanalysis (JRA-25) (Onogi et al. 2007) and the NCEP Climate Forecast System Reanalysis (CFSR), which is a modern reanalysis that should be more comparable with others (Suranjana et al. 2010). Figure 4 also shows an analysis of tropical-wide (30°S–30°N) trends during the period 1979–2005 by Sherwood et al. (2008), who used radiosonde temperature data adjusted to reflect biases and considering the results of applying thermal wind balance to radiosonde-derived winds. The results of applying a MSU TLS-channel weighting (shown on the right side of the left panel) to the San Juan and reanalysis temperatures are also displayed in Fig. 4 and compared with those of the MSU Remote Sensing Systems (RSS), version 3.3, TLS (Mears and Wentz 2009; right panel).

It is clear from Fig. 4 that the original NCEP reanalysis cooling trend from 300 to 100 hPa is excessive compared to that of the San Juan sounding and the other reanalyses and hence likely to be spurious. Overall, the NCEP CFSR and MERRA trends are closest to that of the San Juan radiosonde, whereas the ERA-Interim trend seems too small. At 70 hPa the magnitude of trends from all but the NCEP–NCAR and NCEP CFSR reanalyses are quite small relative to the sonde, whereas NCEP CFSR is very close and NCEP–NCAR is somewhat larger. Nevertheless, this comparison shows evidence from a range of different sources for significant cooling in the region of the TTL (about half as large as in the original NCEP–NCAR reanalysis) that should be expected to influence hurricane outflow temperatures, all other things being equal. It is also clear from the left panel of Fig. 4 that there are very large vertical gradients in the temperature trends across the tropical tropopause layer, with a sharp transition from warming below to cooling above. Thus, small errors in the altitude of the TTL can lead to large errors in trends near 100 hPa. Further, the changes reported in the MSU record are muted by smearing in the vertical (see, e.g., Randel et al. 2009), and the weighting of MSU in some reanalysis data could reflect this.

Analysis of the MSU Temperature Lower Stratosphere (TLS) channel suggests that the downward trend in tropical lower stratospheric temperature over the past few decades is strongest in the North Atlantic region (Fig. 5). This implies that downward trends in outflow temperature should also be largest over the Atlantic. Figure 5 also suggests that TTL cooling over the Atlantic MDR is similar to that at San Juan.

The outflow temperature may be thought of as the absolute temperature at the level at which a parcel saturated as sea surface temperature first loses its positive buoyancy when lifted through the unperturbed environment. Warming sea surface temperature by itself will allow such a parcel to penetrate higher into the TTL and

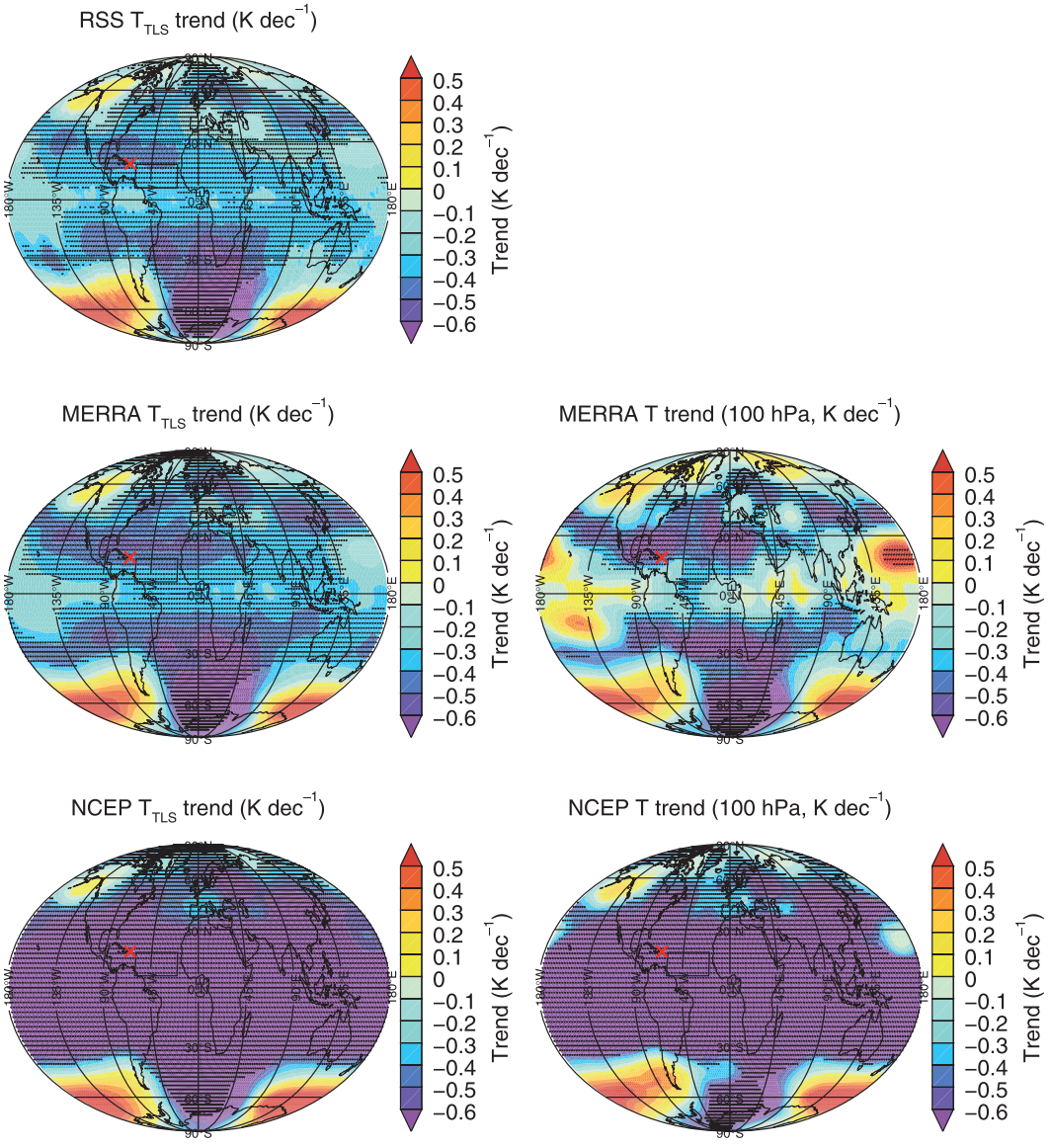

FIG. 5. Geographical patterns of observed and reanalysis trends (K decade^{-1}) in TLS and 100-hPa temperature. All trends are from 1979 to 2011 and averaged over August–October: (left) the TLS trend analyzed from MSU data by (top) RSS and the equivalent trends after applying the TLS channel weighting function to (middle) MERRA and (bottom) NCEP–NCAR temperatures. (right) The reanalysis trends at 100 hPa. The red cross shows the location of San Juan, while the black rectangle outlines the Atlantic MDR.

thus attain a lower temperature; when coupled with any decline in TTL temperature, somewhat larger declines in outflow temperature can occur. For the NCEP–NCAR reanalysis, the outflow temperature declines by 5.4 K while the 100-hPa temperature declines by 4.6 K from 1979 to 2010, while for the San Juan sonde the corresponding numbers are 3.8 and 2.1 K, respectively. Note that, in Figs. 2–4, much of the change in potential intensity and outflow temperature occurred in a single jump around the year 1995. The warming effects of the eruptions of El Chichón in 1982 and Mt. Pinatubo in 1991 are readily apparent.

If the NCEP–NCAR reanalysis data are used, an important part of the increase in tropical cyclone potential intensity over the past few decades is owing to decreasing outflow temperature, with the rest coming from increased thermodynamic disequilibrium at the sea surface. The tropical cyclone downscaling reported by Emanuel et al. (2008) also shows that the increase in potential intensity is largely and perhaps wholly responsible for the increase in

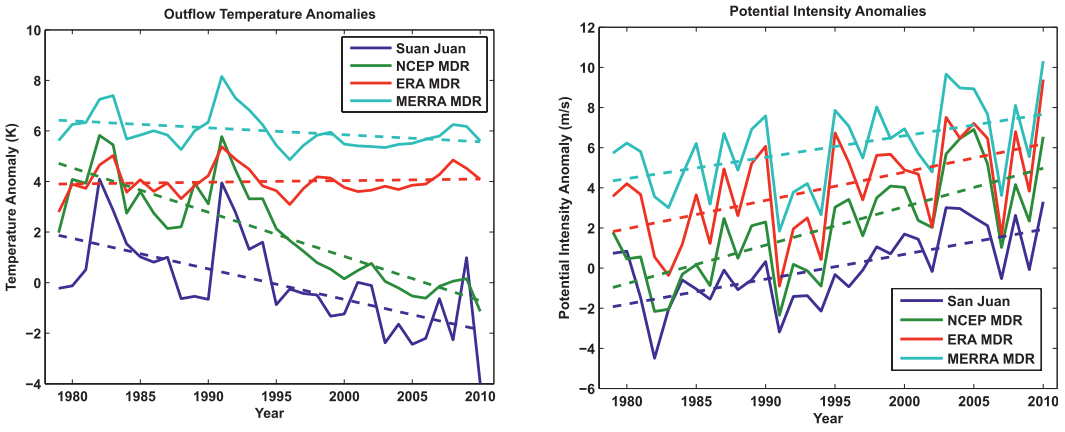

FIG. 6. As in Fig. 3 but showing (left) outflow temperature anomalies and (right) potential intensity anomalies. In the figure at left, 2 K has been added successively to each time series for clarity; at right, 2 m s^{-1} has been added.

Atlantic tropical cyclone activity since the early 1990s. But even with a reduced cooling half as large as in the NCEP–NCAR reanalysis, changes in the TTL would nonetheless play some role in the upswing of Atlantic tropical cyclone activity, discussed further below. For example, the temperature trends at 100 hPa reported by radiosonde would affect calculated trends in outflow temperature and thereby also affect trends in potential intensity, as illustrated in Fig. 6. In constructing this figure, we used RATPAC soundings from San Juan in conjunction with MDR-averaged sea surface temperatures [Hadley Centre Global Sea Ice and Sea Surface Temperature (HadISST); Rayner et al. (2003)] in the potential intensity algorithm of Bister and Emanuel (2002). Figure 6 also shows outflow temperatures and potential intensity changes from three reanalyses. A small part of the differences seen in Fig. 6 may be owing to differences in the sea surface temperatures used by the reanalyses, but examination of time series of these temperatures (not shown) indicates very small differences. The effect of the eruptions of El Chichón and Mt. Pinatubo are again readily apparent in both parts of Fig. 6.

The San Juan sounding indicates potential intensity increases of 1.24 m s^{-1} $decade^{-1}$, compared to rates of 1.92, 1.41, and 1.07 m s^{-1} $decade^{-1}$ for the NCEP–NCAR, ERA-Interim, and MERRA reanalyses, respectively. The rate of increase in NCEP–NCAR-derived potential intensity is about 55% larger than that derived from the San Juan sounding, while that of the MERRA reanalysis is about 14% less. It is apparent in Fig. 6 that the differences in the rates of increase in potential intensity do not always reflect differences in the rates of change of outflow temperature. This is because potential intensity is also controlled by the thermodynamic disequilibrium between the ocean and atmosphere [last term in (6)]. Table 2 shows the contributions to the decadal trends in potential intensity from the last two terms in (6) applied to the San Juan sounding and the three reanalyses. [The sum of the two terms does not equal the trend in potential intensity because (6) is only an approximation to the full algorithm used to calculate the latter.] For the ERA-Interim reanalysis, a large increase in thermodynamic disequilibrium compensates to some extent for the lack of TTL cooling, yielding a reasonably large increase in potential intensity. In the case of the NCEP reanalysis, TTL cooling contributes about half of the total increase in potential intensity, while it contributes about 17% of the total increase from the MERRA reanalysis.

To further explore the influence of TTL cooling on tropical cyclones, we downscale each of the aforementioned reanalyses by generating from the model output large sets of synthetic tropical cyclone events using the downscaling technique of Emanuel et al. (2008). This technique applies a highly resolved, coupled ocean–atmosphere model phrased in angular momentum coordinates (Emanuel 1995) to tracks initiated by random

TABLE 2. Contributions to the decadal trend in potential intensity (m s^{-1} $decade^{-1}$) from the last two terms in (6) for San Juan and each of the three reanalyses, averaged over the Atlantic MDR, August–October.

	San Juan	NCEP	ERA-Interim	MERRA
Contribution from outflow T trend	0.60	0.95	−0.03	0.15
Contribution from trend in thermodynamic disequilibrium	0.91	0.96	1.35	0.71
Sum	1.51	1.91	1.32	0.86
Full trend	1.24	1.92	1.41	1.07

seeding in space and time,[4] and propagated forward using a beta-and-advection model driven by winds derived from the atmospheric general circulation model (AGCM) simulations. The intensity model is integrated along each track. In practice, a large majority of the events suffer declining intensity from their onset and are discarded; the survivors constitute the tropical cyclone climatology of the model.

The downscaling model relies on large-scale winds both to drive the beta-and-advection track model and for deriving wind shear that is input to the intensity model. As described in Emanuel et al. (2006), the winds are derived from synthetic time series of winds constrained to have the same monthly means as those produced by the global model, as well as the same monthly mean covariances among the wind components at two model levels where the fluctuations are defined in terms of departures of daily means from monthly means. The wind time series are also constrained to have power spectra that fall off with the cube of the frequency. The thermodynamic input to the intensity model consists of monthly mean potential intensity and 600-hPa temperature and relative humidity derived from the global models. The ocean component of the intensity model requires ocean mixed layer depth and sub-mixed-layer thermal stratification; in the simulations described here we use present-day climatology for both of these quantities. Thus the effect of global warming on the thermal stratification of the upper ocean is not considered here. When driven by NCEP–NCAR reanalyses during the period 1980–2006, this downscaling technique produces results that explain as much of the observed variance in North Atlantic tropical cyclone activity as do certain global models (LaRow et al. 2008; Zhao et al. 2009a) and the regional downscaling technique of Knutson et al. (2007), which was also driven by NCEP–NCAR reanalysis data. The technique captures well the observed spatial and seasonal variability of tropical cyclones around the globe, as well as the effects of such climate phenomena as ENSO and the Atlantic meridional mode. Thus there are objective reasons to have some confidence in the ability of the downscaling technique to simulate the effects of climate and climate change on tropical cyclone activity.

As might be expected based on the potential intensity trends shown in Fig. 6, the downscaled power dissipation indices of North Atlantic tropical cyclones differ among the three reanalyses (Fig. 7). None of the three exhibits a rate of increase as large as the observed increase of 20% decade^{-1}; the downscaled NCEP–NCAR rate is

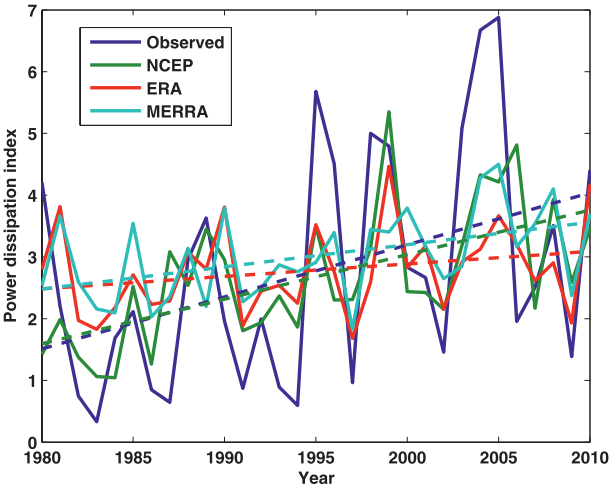

FIG. 7. Annual PDI (10^{11} m^3 s^{-2}) from the National Hurricane Center North Atlantic hurricane database (HURDAT) (blue) and downscaled from the three reanalysis datasets (green, red, and aqua). Dashed lines show the linear trends.

17% decade^{-1}, while ERA-Interim and MERRA yield 9.6% and 11.9% decade^{-1}, respectively.[5] (None of the three reanalyses captures the very exceptional 2005 season; omitting it yields an observed rate of 18% decade^{-1}.) Other tropical cyclone metrics, such as storm frequency, yield similar signals: Only activity downscaled from the NCEP–NCAR reanalysis shows increases similar to those observed. Given that most of the downscaled NCEP–NCAR increase is owing to the increase in potential intensity (Emanuel et al. 2008), it is plausible that the failure of the downscaling of the other two reanalyses to reproduce the observed increase is traceable to the lower magnitudes of their increases in potential intensity (Fig. 6 and Table 2), which are in turn partially attributable to their relatively small TTL cooling. Note that the downscaled power dissipation from MERRA shows a larger upward trend than does that from the ERA-Interim in spite of the fact that the ERA potential intensity trend is larger (Table 2). This is because the two other factors that influence genesis frequency, vertical wind shear and χ as given by (5), both have more favorable trends in the ERA reanalysis than in MERRA. Also note that the influence of El Chichón and Mt. Pinatubo, so clear in Fig. 6, is less so in the observed and downscaled power dissipation, perhaps because of variability that arises from other factors such as χ and shear. But the volcanic signal is somewhat more

[4] Seeding is not done poleward of 75°N or 65°S, or equatorward of 3°.

[5] The ERA-Interim rate has an associated p value of 0.16, so it is of dubious statistical significance. The p values associated with the observed, NCEP–NCAR, and MERRA regressions are 0.02, 3×10^{-4}, and 0.02, respectively.

TABLE 3. Atmospheric general circulation models used in this study.

AGCM	Institution	Reference	Period of integration
CAM3	National Center for Atmospheric Research	Ammann et al. (2007)	850–1999
CAM3 with slab ocean (hereafter, CAM3s)	National Center for Atmospheric Research	Collins et al. (2006)	1979–98
ECHAM5	Max Planck Institute for Meteorology	Roeckner et al. (2006)	1870–2005
GFDL AM2.1	NOAA Geophysical Fluid Dynamics Laboratory	Anderson et al. (2004)	1980–2004
GFDL HiRAM	NOAA Geophysical Fluid Dynamics Laboratory	Zhao et al. (2009)	1982–2007
NOAA Twentieth Century Reanalysis, version 2	NOAA Earth System Research Laboratory	Compo et al. (2011)	1891–2008
MA-ECHAM5 (or MAECHAM)	Max Planck Institute for Meteorology	Roeckner et al. (2006) Manzini et al. (2006) Cagnazzo et al. (2007)	1950–2007

apparent in other metrics of Atlantic tropical cyclone activity (Evan 2012).

4. Absence of TTL cooling in general circulation models and consequences for downscaled tropical cyclones

A well-known bias of most current general circulation models (GCMs) is their failure to capture the cooling of the lower stratosphere and tropical tropopause layer over the past several decades (Cordero and Forster 2006; Gettelman et al. 2010). This is also evident in Fig. 5, which compares the TLS trend averaged over several models with observed MSU trends as deduced by several independent groups. Here we examine the evolution of Atlantic MDR-averaged quantities in six atmospheric GCMs driven by observed sea surface temperature and sea ice cover. A seventh simulation uses an atmospheric GCM coupled to a slab ocean. We also examine tropical cyclones downscaled from these models. The models and their main reference sources are listed in Table 3. Unfortunately, not all of the output variables that we use for diagnosis in this paper were available from all models in the CMIP archive; in what follows, we use all of the models that produced the relevant variables. It should also be noted that these simulations differ in important respects, including their inclusion or lack thereof of volcanic aerosols, variable ozone, and changing CO_2 concentrations.

Figure 8 (left) shows the outflow temperatures calculated from the four models from which it was available and compares them with that calculated from the San Juan RATPAC soundings and MDR-averaged sea surface temperatures (as in the previous section). While all of the models exhibit slight downward trends, only the Community Atmosphere Model, version 3 (CAM3), simulation comes close to the ~1.2 K decade^{-1} drop in outflow temperature calculated from the San Juan soundings.

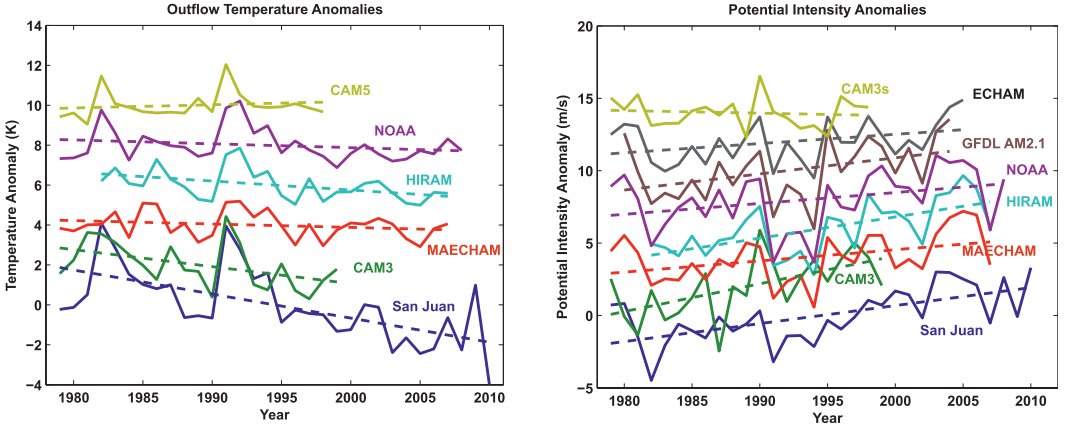

FIG. 8. MDR-averaged (left) outflow temperatures and (right) potential intensities averaged over the period August–October from San Juan soundings (blue) and for subsets of the AGCMs listed in Table 2, depending on availability of the variables. Each successive time series is offset by 2 K and 2 m s^{-1}. Dashed lines show linear regression slopes.

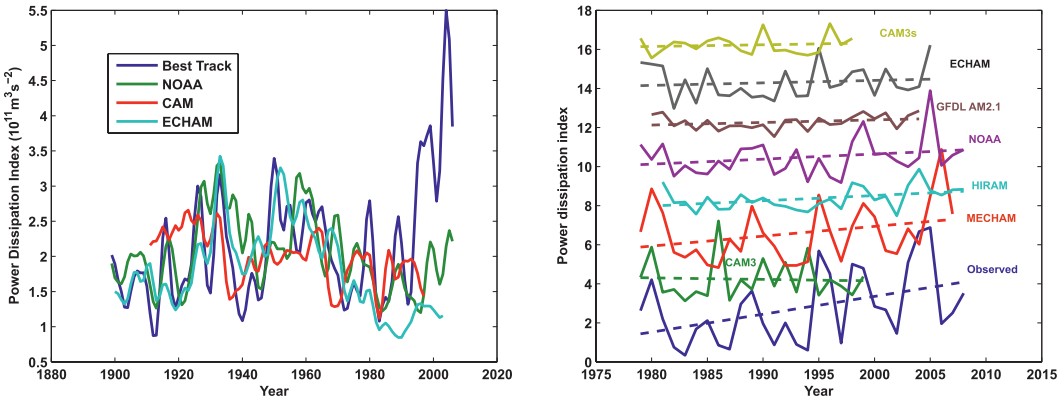

FIG. 9. Annual power dissipation of North Atlantic tropical cyclones downscaled from AGCMs using the technique of Emanuel et al. (2008). (left) The results of the longer model runs; these are compared with estimated actual tropical cyclone power dissipation. (right) The downscaled annual power dissipation from these as well as from the shorter simulations. The longer series at left have been smoothed in time using a 1–3–4–3–1 filter. Series at right have been displaced from each other by 2×10^{11} m^3 s^{-2} for clarity. The right panel also shows linear regression slopes (dashed lines) of the time series.

Since all of the models and the reanalyses use virtually the same sea surface temperatures, the failure of the AGCMs to simulate the drop in outflow temperature is likely rooted in their failure to simulate the decline in TTL and lower stratosphere temperatures, as documented by Thompson and Solomon (2005), Cordero and Forster (2006), Gettelman et al. (2010), and others (also see Fig. 5). Modeled 100-hPa temperature trends show around 0.3 K^{-1} decade^{-1} less cooling over the period 1979–2005 than those inferred from rawinsonde winds using the thermal wind equation (Allen and Sherwood 2008). The absence of clear volcanic signatures in the MAECHAM time series is owing to the absence of volcanic aerosols in that simulation.

The failure of the AGCMs to capture the TTL cooling is to some extent reflected in the evolution over time of the MDR-averaged potential intensities calculated from monthly mean output of the AGCMs, also averaged over the period August–October (Fig. 8, right). While all of the models' potential intensities show upward trends, only CAM3, GFDL HiRAM, and GFDL AM2.1 have trends as large as that inferred from the San Juan soundings. (The CAM3 trend is actually somewhat larger but extends over a shorter interval; when compared over the same intervals, the trends are quite similar.) Although the HiRAM outflow temperature does not decrease as fast as that based on the San Juan sounding, its potential intensity increases at about the same rate thanks to a faster increase in air–sea thermodynamic disequilibrium over this time interval.

Figure 9 shows the results of downscaling the models listed in Table 2. Some of the models that were run for many decades are shown on the left, while those that were run beginning after 1979 are shown on the right; both are compared with the National Hurricane Center best-track data (Jarvinen et al. 1984) as corrected for overestimation of wind speeds prior to 1970, based on Landsea (1993).

It is clear from Fig. 9 that, while the downscaled tropical cyclone power dissipation is in reasonable agreement with the historical record before roughly 1980, none of the models fully captures the large and well-documented increase in Atlantic tropical cyclone power dissipation after the early 1990s. On the other hand, the downscaled NCEP–NCAR reanalysis shows quite good agreement with historical data, as had been reported previously by Emanuel et al. (2008). The two atmospheric thermodynamic variables that influence the simple intensity model used in the downscaling are the potential intensity and χ as defined by (5). (Constant monthly mean climatological values are used for upper-ocean mixed layer depth and sub-mixed-layer thermal stratification.) In most of these simulations, χ decreases after about 1990, so potential intensity is the only remaining thermodynamic factor that can explain changes in downscaled tropical cyclone activity during this period.

The results of this analysis are summarized in Fig. 10, which graphs the difference between downscaled and observed trends in annual tropical cyclone power dissipation (1979 and after) against the difference between modeled outflow temperature and that inferred from the San Juan soundings for all of the models and reanalysis products for which the outflow temperature was available. Larger differences in outflow temperature trends are accompanied by larger errors in downscaled power dissipation trends. This demonstrates that errors in TTL temperature trends are associated with errors in

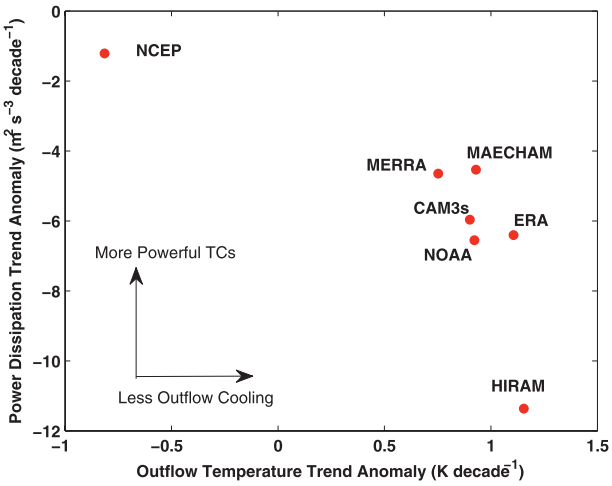

FIG. 10. Difference between linear regression slopes of downscaled power dissipation and observed events over the same period of time graphed against the difference between the regression slopes of modeled and reanalyzed outflow temperature and that inferred from San Juan soundings over the same period of time. Note that the various model trends are, in general, over somewhat different periods of time (see right-hand side of Fig. 9).

downscaled tropical cyclone trends. In the next section we will briefly review what is known about the causes of TTL and lower stratosphere cooling and its implications for tropical cyclones in a future climate.

5. Causes and implications of TTL cooling

Evidence for cooling of the lower stratosphere over the past few decades is supported by analysis of several different measurement systems, including rawinsonde temperatures (Thompson and Solomon 2005; Gettelman et al. 2010) and satellite-borne microwave sounding unit-derived temperatures (Fu et al. 2006). Temperature trends derived from rawinsonde winds using balance relationships (Allen and Sherwood 2008) also show pronounced cooling with a sharp gradient from warming to cooling across the tropical TTL. The cooling is evident at all latitudes (Randel et al. 2009), and there is some evidence that its magnitude is spatially inversely correlated with upper tropospheric warming (Fu et al. 2006; Rosenlof and Reid 2008). The cooling has not been uniform in time but seems to have occurred largely in two steps corresponding to the eruptions of El Chichón in 1982 and Mt. Pinatubo in 1991 (Ramaswamy et al. 2006; Thompson and Solomon 2009).

Various mechanisms have been proposed to account for the cooling. The tropical lower stratosphere normally has temperatures well below radiative equilibrium, owing to adiabatic cooling associated with the Brewer–Dobson circulation; it seems reasonable to assume that any enhancement of Brewer–Dobson overturning should lead to additional cooling. There is some evidence that secular increases in the Brewer–Dobson circulation have occurred in recent decades (Thompson and Solomon 2005; Deckert and Dameris 2008; Garcia and Randel 2008; Thompson and Solomon 2009; Fu et al. 2010) and that global climate change may lead to further acceleration of the circulation and associated cooling of the lower tropical stratosphere (Garcia and Randel 2008; Gettelman et al. 2009; McLandress and Shepherd 2009). A factor influencing the cooling is ozone loss (Forster et al. 2007). Ozone loss in this region in turn is likely to have resulted from increased upwelling of ozone-poor air from the troposphere, so it may prove difficult to distinguish observationally between the direct adiabatic cooling and ozone loss, both of which result from increased upwelling (Thompson and Solomon 2009). The record of lower stratospheric temperature change over the past three decades, together with an analysis of models, suggests that the main influences have been a slow secular cooling owing to increasing magnitude of the Brewer–Dobson circulation, but with strong influences from the two major volcanic eruptions of this period. Volcanoes initially heat the lower stratosphere through the radiative effects of volcanic aerosols, but aerosol particles produced from volcanic gases interact with atmospheric chlorine to produce longer-term ozone depletion, tending to produce a cooling signal that follows the aerosol-induced warming (Thompson and Solomon 2009).

Understanding the causes of the observed cooling is vital for making accurate projections of TTL temperature, especially given the failure of global climate models to adequately simulate the cooling (Cordero and Forster 2006; Gettelman et al. 2010). In view of the effect of TTL cooling on tropical cyclones, the failure of global models to capture the cooling suggests that their current ability to predict future changes in tropical cyclone activity may be compromised. Insofar as reanalyses depend upon both observations and forcing, any shortcomings in representing ozone losses or the processes controlling the strength of the Brewer–Dobson circulation and its changes can also influence reanalyses.

6. Summary

Tropical cyclones are sensitive to both their kinematic and thermodynamic environments. Discussions of the latter usually focus on sea surface temperature (absolute or relative) as the thermodynamic quantity most relevant to tropical cyclones. Here we emphasize that the relevant thermodynamic quantities are the air–sea thermodynamic disequilibrium and thermodynamic efficiency, which control potential intensity; surface enthalpy flux,

which contributes to convective activity; and mid-tropospheric saturation deficit, which has a strong effect both on convection and on tropical cyclone development. At least in the North Atlantic region, where recent trends appear to be dominated by thermodynamic influences, downward trends in tropical cyclone outflow temperature, associated with a cooling tropical tropopause layer and lower stratosphere, are a significant contributor to upward trends in potential intensity over the past few decades, at least as inferred from time series of soundings at San Juan, Puerto Rico, and from NCEP–NCAR and MERRA reanalyses. Application of a tropical cyclone downscaling technique to NCEP–NCAR and MERRA reanalysis data implies that TTL cooling has made a significant contribution to the increase in tropical cyclone activity over this period, but comparisons with MSU and sounding data suggests that the NCEP–NCAR reanalysis overestimates the cooling and, therefore, the increase in potential intensity. The uncertainties in temperature changes in this region are hence of great importance for attempts to interpret tropical cyclone changes. In this regard it is important to emphasize the evident role played by several past volcanic eruptions in modulating temperatures in and around the TTL so that it is not just long-term trends that need to be considered but also shorter-term episodic changes. It is well known that most global circulation models underestimate this cooling and, when the downscaling technique is applied to such models, they largely fail to capture the observed increase in North Atlantic tropical cyclone activity. Extant work suggests that the observed cooling of the tropical TTL and lower stratosphere since 1979 is linked not only to warming by major volcanic eruptions in the first 15 years of the record but also to a combination of ozone depletion and increased Brewer–Dobson upwelling. The failure of most GCMs to capture this cooling must be addressed before such models can be used to project future changes in tropical cyclone activity.

Acknowledgments. The authors thank Michael Mann, Michael Kozar, Caspar Ammann, and Bette Otto-Bleisner for providing the CAM3 model output, and Natalie Mahowald and Amato Evan for output from the slab ocean version of CAM3. We thank Ming Zhao of NOAA/GFDL for providing output of the GFDL HiRAM model. ECHAM5-HAM computations were performed at the Swiss National Supercomputing Center (CSCS). We also thank David Raymond, Jim Kossin, and an anonymous reviewer for constructive comments that led to significant improvement of the original manuscript. DF was financially supported by the National Centers for Competence in Research (NCCR) in the context of the HyClim project. The first author's contributions were supported by the National Science Foundation under Grant AGS-0850639.

REFERENCES

Allen, R. J., and S. C. Sherwood, 2008: Warming maximum in the tropical upper troposphere deduced from thermal winds. *Nat. Geosci.,* **1,** 399–403, doi:10.1038/ngeo208.

Ammann, C. M., F. Joos, D. S. Schimel, B. L. Otto-Bliesner, and R. A. Tomas, 2007: Solar influence on climate during the past millennium: Results from transient simulations with the NCAR Climate System Model. *Proc. Natl. Acad. Sci. USA,* **104,** 3713–3718.

Anderson, J. L., and Coauthors, 2004: The new GFDL global atmosphere and land model AM2–LM2: Evaluation with prescribed SST simulations. *J. Climate,* **17,** 4641–4673.

Bister, M., and K. A. Emanuel, 1998: Dissipative heating and hurricane intensity. *Meteor. Atmos. Phys.,* **65,** 233–240.

——, and ——, 2002: Low frequency variability of tropical cyclone potential intensity, 1: Interannual to interdecadal variability. *J. Geophys. Res.,* **107,** 4801, doi:10.1029/2001JD000776.

Bryan, G. H., and R. Rotunno, 2009: Evaluation of an analytical model for the maximum intensity of tropical cyclones. *J. Atmos. Sci.,* **66,** 3042–3060.

Cagnazzo, C., E. Manzini, M. A. Giorgetta, P. M. D. F. Forster, and J. J. Morcrette, 2007: Impact of an improved shortwave radiation scheme in the MAECHAM5 general circulation model. *Atmos. Chem. Phys.,* **7,** 2503–2515.

Collins, W. D., and Coauthors, 2006: The formulation and atmospheric simulation of the Community Atmosphere Model version 3 (CAM3). *J. Climate,* **19,** 2144–2161.

Compo, G. P., and Coauthors, 2011: The Twentieth Century Reanalysis Project. *Quart. J. Roy. Meteor. Soc.,* **137,** 1–28.

Cordero, E. C., and P. M. Forster, 2006: Stratospheric variability and trends in models used for the IPCC AR4. *Atmos. Chem. Phys.,* **6,** 5369–5380.

Deckert, R., and M. Dameris, 2008: Higher tropical SSTs strengthen the tropical upwelling via deep convection. *Geophys. Res. Lett.,* **35,** L10813, doi:10.1029/2008GL033719.

Dee, D. P., and Coauthors, 2011: The ERA-Interim reanalysis: Configuration and performance of the data assimilation system. *Quart. J. Roy. Meteor. Soc.,* **137,** 553–597.

Emanuel, K. A., 1995: The behavior of a simple hurricane model using a convective scheme based on subcloud-layer entropy equilibrium. *J. Atmos. Sci.,* **52,** 3959–3968.

——, 2005: Increasing destructiveness of tropical cyclones over the past 30 years. *Nature,* **436,** 686–688.

——, and R. Rotunno, 2011: Self-stratification of tropical cyclone outflow. Part I: Implications for storm structure. *J. Atmos. Sci.,* **68,** 2236–2249.

——, S. Ravela, E. Vivant, and C. Risi, 2006: A statistical deterministic approach to hurricane risk assessment. *Bull. Amer. Meteor. Soc.,* **19,** 299–314.

——, R. Sundararajan, and J. Williams, 2008: Hurricanes and global warming: Results from downscaling IPCC AR4 simulations. *Bull. Amer. Meteor. Soc.,* **89,** 347–367.

Evan, A. T., 2012: Atlantic hurricane activity following two major volcanic eruptions. *J. Geophys. Res.,* **117,** D06101, doi:10.1029/2011JD016716.

Forster, P. M., G. Bodeker, R. Schofield, S. Solomon, and D. Thompson, 2007: Effects of ozone cooling in the tropical lower stratosphere and upper troposphere. *Geophys. Res. Lett.,* **34,** L23813, doi:10.1029/2007GL031994.

Fu, Q., C. M. Johanson, J. M. Wallace, and T. Reichler, 2006: Enhanced mid-latitude tropospheric warming in satellite measurements. *Science,* **312,** 1179.

——, S. Solomon, and P. Lin, 2010: On the seasonal dependence of tropical lower-stratospheric temperature trends. *Atmos. Chem. Phys.,* **10,** 2643–2653.

Garcia, R. R., and W. J. Randel, 2008: Acceleration of the Brewer–Dobson circulation due to increases in greenhouse gases. *J. Atmos. Sci.,* **65,** 2731–2739.

Gettelman, A., and Coauthors, 2009: The tropical tropopause layer 1960–2100. *Atmos. Chem. Phys.,* **9,** 1621–1637.

——, and Coauthors, 2010: Multimodel assessment of the upper troposphere and lower stratosphere: Tropics and global trends. *J. Geophys. Res.,* **115,** D00M08, doi:10.1029/2009JD013638.

Jarvinen, B. R., C. J. Neumann, and M. A. S. Davis, 1984: A tropical cyclone data tape for the North Atlantic Basin, 1886–1983: Contents, limitations, and uses. NOAA Tech. Memo. NWS NHC 22, 21 pp.

Knutson, T. R., J. J. Sirutis, S. T. Garner, I. M. Held, and R. E. Tuleya, 2007: Simulation of the recent multi-decadal increase of Atlantic hurricane activity using an 18-km grid regional model. *Bull. Amer. Meteor. Soc.,* **88,** 1549–1565.

——, and Coauthors, 2010: Tropical cyclones and climate change. *Nat. Geosci.,* **3,** 157–163.

Landsea, C., 1993: A climatology of intense (or major) Atlantic hurricanes. *Mon. Wea. Rev.,* **121,** 1703–1714.

Lanzante, J. R., S. A. Klein, and D. J. Seidel, 2003a: Temporal homogenization of monthly radiosonde temperature data. Part I: Methodology. *J. Climate,* **16,** 224–240.

——, ——, and ——, 2003b: Temporal homogenization of monthly radiosonde temperature data. Part II: Trends, sensitivities, and MSU comparison. *J. Climate,* **16,** 241–262.

LaRow, T. E., L. Stefanova, S.-W. D.-W. Shin, and S. Cocke, 2008: Seasonal Atlantic tropical cyclone hindcasting/forecasting using two sea surface temperature datasets. *Geophys. Res. Lett.,* **37,** L02804, doi:10.1029/2009GL041459.

Manzini, E., M. A. Giorgetta, M. Esch, L. Kornblueh, and E. Roeckner, 2006: The influence of sea surface temperatures on the northern winter stratosphere: Ensemble simulations with the MAECHAM5 model. *J. Climate,* **19,** 3863–3881.

McLandress, C., and T. G. Shepherd, 2009: Simulated anthropogenic changes in the Brewer–Dobson circulation, including its extension to high latitudes. *J. Climate,* **22,** 1516–1540.

Mears, C. A., and F. J. Wentz, 2009: Construction of the Remote Sensing Systems V3.2 atmospheric temperature records from the MSU and AMSU microwave sounders. *J. Atmos. Oceanic Technol.,* **26,** 1404–1056.

Onogi, K., and Coauthors, 2007: The JRA-25 reanalysis. *J. Meteor. Soc. Japan,* **85,** 369–432.

Ramaswamy, V., M. Schwarzkopf, W. J. Randel, B. D. Santer, B. J. Soden, and G. L. Stenchikov, 2006: Anthropogenic and natural influences in the evolution of lower stratospheric cooling. *Science,* **311,** 1138–1141, doi:10.1126/science.1122587.

Randel, W. J., and Coauthors, 2009: An update of observed stratospheric temperature trends. *J. Geophys. Res.,* **114,** D02107, doi:10.1029/2008JD010421.

Raymond, D. J., 1995: Regulation of moist convection over the west Pacific warm pool. *J. Atmos. Sci.,* **52,** 3945–3959.

Rayner, N. A., D. E. Parker, E. B. Horton, C. K. Folland, L. V. Alexander, D. P. Rowell, E. C. Kent, and A. Kaplan, 2003: Global analyses of sea surface temperature, sea ice, and night marine air temperature since the late nineteenth century. *J. Geophys. Res.,* **108,** 4407, doi:10.1029/2002JD002670.

Rienecker, M. M., and Coauthors, 2011: MERRA: NASA's Modern-Era Retrospective Analysis for Research and Applications. *J. Climate,* **24,** 3624–3648.

Roeckner, E., and Coauthors, 2006: Sensitivity of simulated climate to horizontal and vertical resolution in the ECHAM5 atmosphere model. *J. Climate,* **19,** 3771–3791.

Rosenlof, K. H., and G. C. Reid, 2008: Trends in the temperature and water vapor content of the tropical lower stratosphere: Sea surface connection. *J. Geophys. Res.,* **113,** D06107, doi:10.1029/2007JD009109.

Sherwood, S. C., C. L. Meyer, R. J. Allen, and H. A. Titchner, 2008: Robust tropospheric warming revealed by iteratively homogenized radiosonde data. *J. Climate,* **21,** 5336–5350.

Smith, R. K., M. T. Montgomery, and S. Vogl, 2008: A critique of Emanuel's hurricane model and potential intensity theory. *Quart. J. Roy. Meteor. Soc.,* **134,** 551–561.

Suranjana, S., and Coauthors, 2010: The NCEP Climate Forecast System Reanalysis. *Bull. Amer. Meteor. Soc.,* **91,** 1015–1057.

Thompson, D. W. J., and S. Solomon, 2005: Recent stratospheric climate trends as evidenced in radiosonde data: Global structure and tropospheric linkages. *J. Climate,* **18,** 4785–4795.

——, and ——, 2009: Understanding recent stratospheric climate change. *J. Climate,* **22,** 1934–1943.

Zhao, M., I. M. Held, S.-J. Lin, and G. A. Vecchi, 2009: Simulations of global hurricane climatology, interannual variability, and response to global warming using a 50-km resolution GCM. *J. Climate,* **22,** 6653–6678.